

Using small baseline Interferometric SAR to map nonlinear ground motion: a case study in Northern Tibet

Zhenhong Li, Yanxiong Liu, Xinghua Zhou, Paul Cross and Wanpeng Feng

Abstract. With its global coverage and all-weather imaging capability, Interferometric SAR (InSAR) has been revolutionizing our ability to image the Earth's surface and the evolution of its shape over time. In turn, this has led to many new insights into geophysical and engineering processes, such as volcanoes, earthquakes, landslides and mining activity. In this study, we used an advanced InSAR time series technique to map ground motion of an area in Northern Tibet using ENVISAT images acquired between 2003 and 2007. In order to minimise the effects of baseline decorrelation, a subset of possible pairs having a perpendicular baseline (i.e. orbital separation) of less than 400 m was chosen for the InSAR time series analysis. The time series results reveal an 'unexpected' nonlinear ground motion: the area of interest was relatively stable during the period from 2003 to the middle of 2004, whilst it has exhibited a nearly linear uplift of about 8 cm since the middle of 2004. Examination of high-resolution ALOS PRISM images shows that the uplift signal occurred over the Huatugou oil field and is most likely caused by water injection. This study highlights the potential of InSAR as an early detection tool of surface deformations.

1. Introduction

Interferometric SAR (InSAR) techniques utilize the phase differences in complex (amplitude and phase) Synthetic Aperture Radar (SAR) images acquired under similar geometric conditions, but at two different epochs, to measure the component of the surface displacement (i.e. range changes) in the direction of the radar line of sight (LOS) with tens-of metres horizontal spatial resolution over large regions (e.g. 100 km × 100 km). With its global coverage and all-weather imaging capability, InSAR has been revolutionizing our ability to image the Earth's surface, which in turn has led to many new insights into geophysical and engineering processes, such as volcanoes, earthquakes, landslides and mining activity (Lu et al. 2007, Massonnet and Feigl 1998).

The original purpose of this study was to map the interseismic motion of the Eastern Altyn Tagh Fault so as to provide evidence for or against the existence of rigid plate deformation in the Tibetan plateau (e.g. Thatcher 2007) using ENVISAT SAR. The interferograms produced generally span about 8 degrees of latitude (i.e. a north-south distance of 888 km). This paper however, focuses on an "unexpected" localized uplift signal over a small area (4.5 km × 2.7 km) re-

vealed by our time series analysis. The main structure of this paper is as follows: A description of the small baseline (SB) InSAR time series technique is given in Section 2. The main InSAR error sources are presented in Section 3, followed by our InSAR time series results and a detailed discussion. In Section 4, we draw our conclusions.

2. Methods

2.1. Phase measurements

After removing the flat earth and local topography, the unwrapped differential interferometric phase at pixel (x, r) (x and r are the azimuth and range coordinates respectively) computed from the SAR acquisitions at times t_M (start time) and t_S (end time) can be written as follows (Berardino et al. 2002):

$$\begin{cases} \delta\phi_{t_M t_S}(x, r) = \delta\phi_{t_M t_S}^{\text{topo}}(x, r) + \delta\phi_{t_M t_S}^{\text{disp}}(x, r) \\ \quad + \delta\phi_{t_M t_S}^{\text{atm}}(x, r) + \delta\phi_{t_M t_S}^{\text{noise}}(x, r), \\ \delta\phi_{t_M t_S}^{\text{topo}}(x, r) = \frac{4\pi}{\lambda} \frac{B_{\perp t_M t_S} \Delta Z(x, r)}{r \sin \theta}, \\ \delta\phi_{t_M t_S}^{\text{disp}}(x, r) = \frac{4\pi}{\lambda} [d(t_S, x, r) - d(t_M, x, r)], \\ \delta\phi_{t_M t_S}^{\text{atm}}(x, r) = \frac{4\pi}{\lambda} [d_{\text{atm}}(t_S, x, r) - d_{\text{atm}}(t_M, x, r)], \end{cases} \quad (1)$$

where λ is the transmitted signal central wavelength in mm (e.g. 56.3 mm for ASAR, and 236 mm for ALOS PALSAR), $d(t_S, x, r)$ and $d(t_M, x, r)$ respectively represent the cumulative deformation in the line of sight at times t_S and t_M with respect to the reference time t_0 , i.e. implying $d(t_0, x, r) = 0$ for all (x, r) ; $\Delta Z(x, r)$ is the topographic error present in the DEM used for interferogram generation, its impact on deformation maps is a function of the perpendicular baseline component $B_{\perp t_M t_S}$, the sensor-target distance r , and the look angle θ . The terms $d_{\text{atm}}(t_M, x, r)$ and $d_{\text{atm}}(t_S, x, r)$ account for temporal atmospheric variations at pixel (x, r) , and the final term $\delta\phi_{t_M t_S}^{\text{noise}}(x, r)$ for temporal decorrelation, orbital errors and thermal noise effects.

In equation (1), it is clear that the smaller the perpendicular baseline, the less the impact of DEM errors on a deformation map. Assuming a nominal incidence angle of 23° and a perpendicular baseline of 100 m, the typical topographic errors in the SRTM DEM (8.7 m in Eurasia (Farr et al. 2007)) might lead to a phase error of 0.61 rad, which is well below the typical phase noise level of the InSAR pairs, on the order of ~ 0.70 rad (Hanssen 2001). Therefore,

the topographic contribution can be considered negligible for InSAR pairs with a perpendicular baseline of 100 m or shorter (see more details in Section 3.1).

Atmospheric effects were first identified in repeat-pass InSAR measurements by (Massonnet et al. 1994) when they studied the 1992 Landers earthquake. Zebker et al. (1997) suggested that a 20% spatial or temporal change in relative humidity could result in a 10–14 cm error in deformation measurement retrievals, independent of any baseline parameter. It should be noted that the atmospheric phase component in equation (1) also includes ionospheric effects (Hanssen 2001). However, because the occurrence of phase scintillation due to small-scale ionospheric disturbances is limited in the equatorial and auroral regions, and extremely rare in mid-latitude regions; and ionospheric effects on InSAR measurements should be ~ 17 times less at C-band than at L-band, an assumption is made in this paper that ionospheric effects will not significantly affect phase variations in C-band SAR images, although they may lead to long wavelength gradients which can be removed using a best-fit plane (Massonnet and Feigl 1998).

2.2. InSAR time series (InSAR TS)

Over the past few years, reduction of atmospheric effects on InSAR measurements have been successfully demonstrated using independent water vapour measurements (Ding et al. 2008), e.g. GPS (Janssen et al. 2004, Li et al. 2006a, Li et al. 2004, Onn and Zebker 2006, Xu et al. 2006), the NASA Moderate Resolution Imaging Spectroradiometer (MODIS) (Li et al. 2005) and the ESA Medium Resolution Imaging Spectrometer (MERIS) (Li et al. 2006b, Li et al. 2006c). After water vapour correction, atmospheric effects on the corrected interferograms are limited and their residuals can be considered as random noise, so that $\delta\phi_{t_M t_S}^{\text{atm}}(x, r) = \text{ZPDDM} + \delta\phi_{t_M t_S}^{\text{residual}}(x, r)$ (where ZPDDM is Zenith Path Delay Difference Map (Li et al. 2006a, Li et al. 2009b, Li et al. 2005)) can be cancelled out in equation (1):

$$\begin{cases} \delta\phi_{t_M t_S}^{\text{corr}}(x, r) = \delta\phi_{t_M t_S}^{\text{topo}}(x, r) + \delta\phi_{t_M t_S}^{\text{disp}}(x, r) \\ \quad + \delta\phi_{t_M t_S}^{\text{noise}^2}(x, r), \\ \delta\phi_{t_M t_S}^{\text{corr}}(x, r) = \delta\phi_{t_M t_S}(x, r) - \text{ZPDDM}_{t_M t_S}, \\ \delta\phi_{t_M t_S}^{\text{noise}^2}(x, r) = \delta\phi_{t_M t_S}^{\text{noise}}(x, r) + \delta\phi_{t_M t_S}^{\text{residual}}(x, r), \end{cases} \quad (2)$$

where $\delta\phi_{t_M t_S}^{\text{corr}}(x, r)$ represents corrected phase values and $\delta\phi_{t_M t_S}^{\text{residual}}(x, r)$ residual water vapour effects after correction.

The small baseline subset algorithm (SBAS) is a robust InSAR time series analysis approach, which uses interferograms with small baselines to minimize the effects of baseline decorrelation and inaccuracies in topographic data used (Berardino et al. 2002, Casu et al. 2006, Lanari et al. 2007, Lanari et al. 2004). As shown in Figure 1, let t be a vector of SAR acquisition dates in chronological order. For

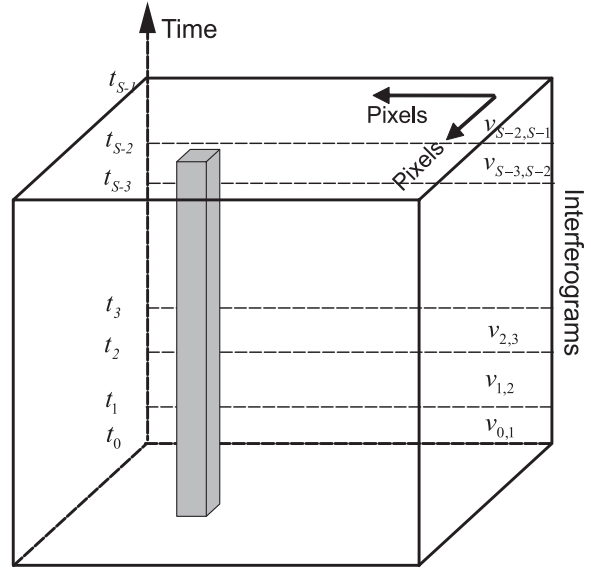


Figure 1: InSAR time series schematic.

a dataset containing N interferograms constructed from S acquisitions on different dates, assuming $v_{k,k+1}$ is the mean velocity between the time-adjacent (e.g. the k th and $(k+1)$ th time) acquisitions, the deformation phase can be written as (Berardino et al. 2002):

$$\begin{aligned} \delta\phi_{t_M t_S}^{\text{disp}}(x, r) &= \frac{4\pi}{\lambda} [d(t_S, x, r) - d(t_M, x, r)] \\ &= \frac{4\pi}{\lambda} \sum_{k=M}^{S-1} v_{k,k+1} (t_{k+1} - t_k). \end{aligned} \quad (3)$$

For a given pixel, let V be a vector (of size $(S-1) \times 1$) of successive velocities (i.e. $V^T = [v_{0,1} \ v_{1,2} \ \dots \ v_{S-2,S-1}]$), Z a parameter of DEM errors, and R a vector of interferogram range changes in the line of sight (of size $N \times 1$). Equation (2) can be generalized into a matrix equation for the entire set of interferograms (Berardino et al. 2002):

$$\begin{cases} \begin{bmatrix} T & C \\ N \times (S-1) & N \times 1 \end{bmatrix} \begin{bmatrix} V \\ Z \\ 1 \times 1 \end{bmatrix} = \begin{bmatrix} R \\ N \times 1 \end{bmatrix}, \\ C^T = \begin{bmatrix} \frac{B_{\perp 1}}{r \sin \theta} & \frac{B_{\perp 2}}{r \sin \theta} & \dots & \frac{B_{\perp N}}{r \sin \theta} \end{bmatrix}, \\ R^T = \begin{bmatrix} \frac{\lambda}{4\pi} \delta\phi_1^{\text{corr}} & \frac{\lambda}{4\pi} \delta\phi_2^{\text{corr}} & \dots & \frac{\lambda}{4\pi} \delta\phi_N^{\text{corr}} \end{bmatrix}, \end{cases} \quad (4)$$

where the $N \times (S-1)$ matrix T references the time interval of each interferogram, e.g.

$$T_{N \times (S-1)} = \begin{bmatrix} t_1 - t_0 & t_2 - t_1 & 0 & \dots & \dots & 0 \\ 0 & t_2 - t_1 & t_3 - t_2 & 0 & \dots & 0 \\ \dots & \dots & \dots & \dots & \dots & \dots \\ 0 & 0 & \dots & \dots & t_{S-2} - t_{S-3} & t_{S-1} - t_{S-2} \end{bmatrix}. \quad (5)$$

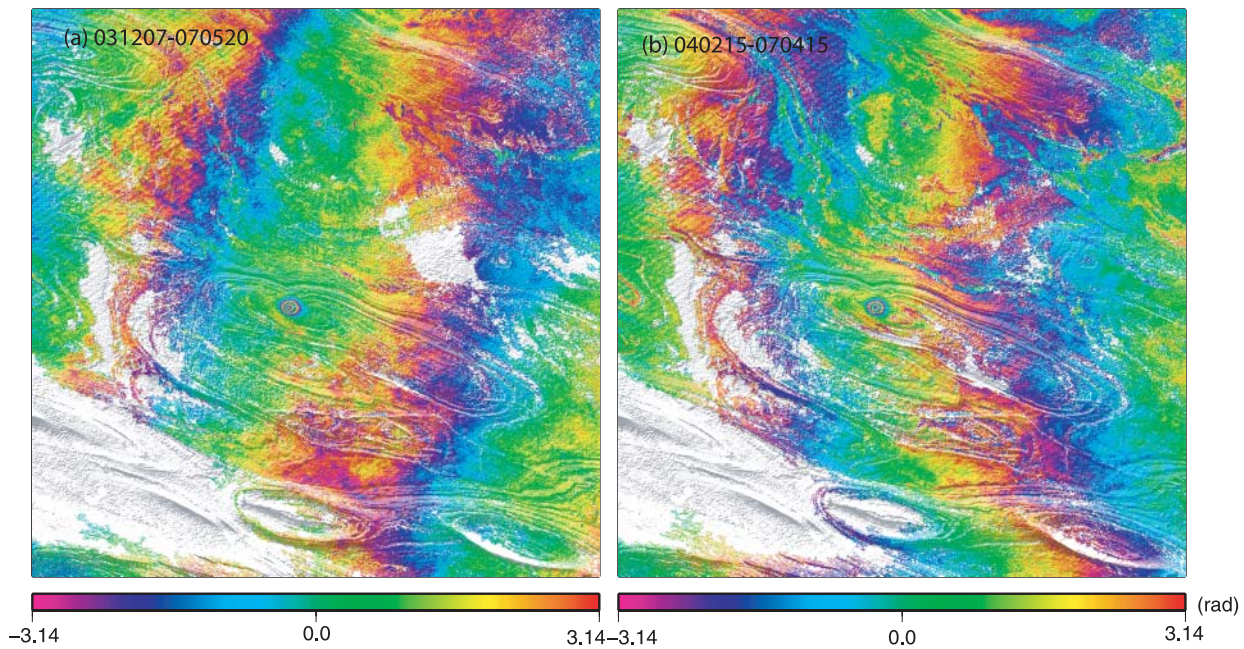


Figure 4: Orbital ramps: (a) 031207-070520; (b) 040215-070415.

long baselines are required in the InSAR time series to form a connected network. Therefore, to obtain a reliable deformation time series, height errors are estimated in the InSAR TS for each pixel, bearing in mind their sensitivity to the perpendicular baseline length.

Orbital ramp. The knowledge of satellite orbits is limited; it is believed that a realistic total orbit error of around 10 cm is applicable to ENVISAT, with radial accuracy being around 3 cm (Otten and Dow 2004). After known geometrical contributions have been removed using precise orbits, residual phase ramps remain in interferograms. In northern Tibet, orbital

ramps can be easily observed even in a small region (e.g. two fringes in an area of $53 \text{ km} \times 66 \text{ km}$, Figures 3(b) and 4). A conventional way to reduce orbital errors is to subtract a best-fit plane or quadratic surface directly from the unwrapped phase. Note that this approach may also remove the long-wavelength component of deformation signals. The signals of interest in this paper are localised, and therefore this approach should be sufficiently accurate.

Phase unwrapping error. Interferometric phase measurements are modulo 2π radians, and a fringe is equivalent to ground motion of half the radar wavelength (e.g. 2.8 cm for the Envisat satellite) in the sat-

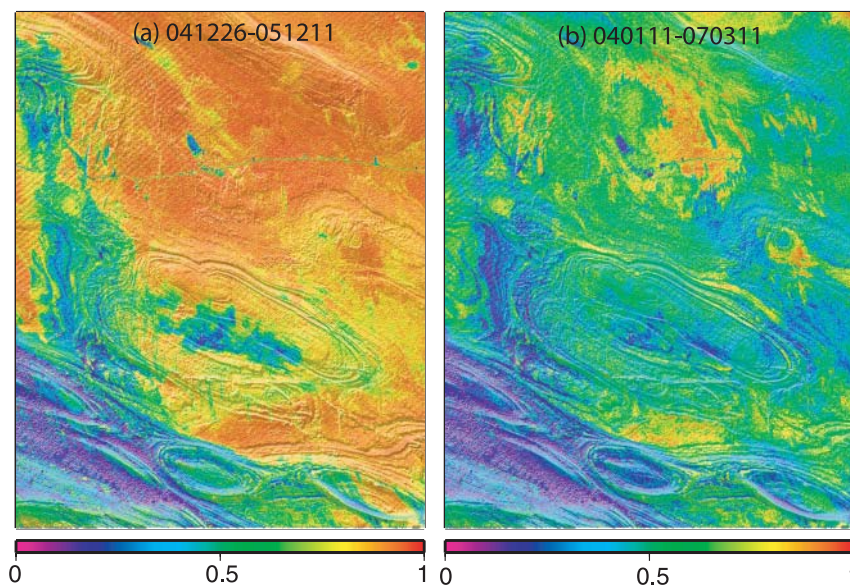


Figure 5: Examples of interferometric coherence maps over the area of interest: (a) 041226-051211 (spanning about 1 year); (b) 040111-070311 (spanning 3 years and 2 months).

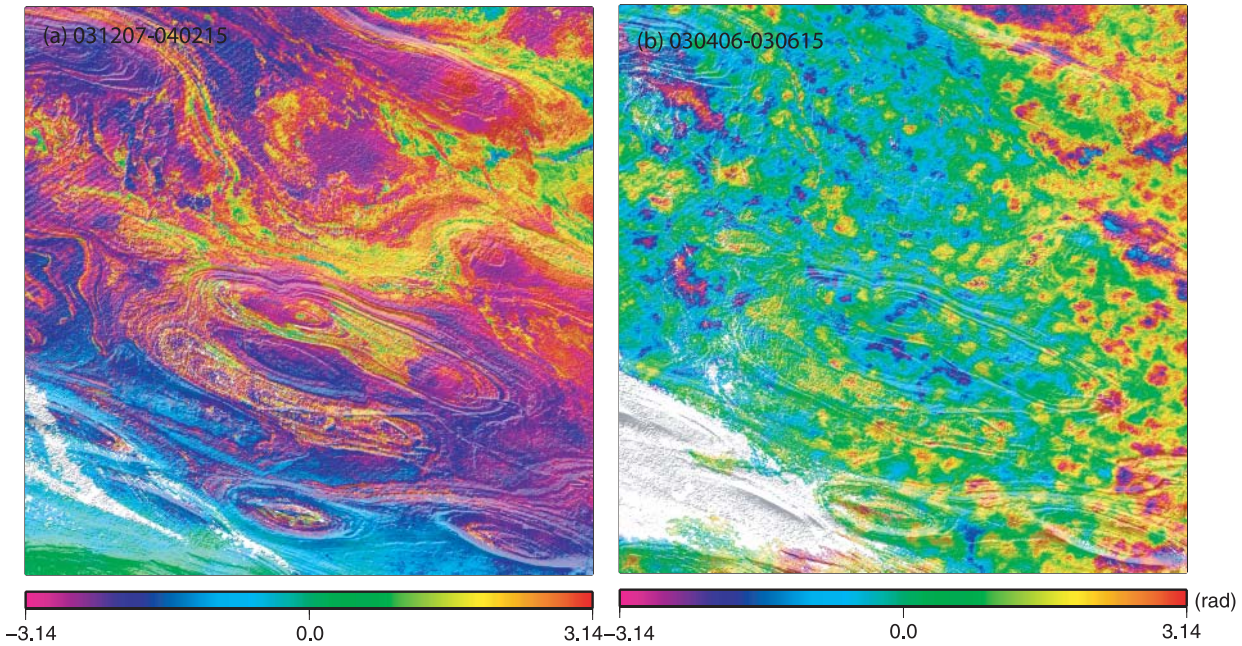


Figure 6: InSAR atmospheric effects: (a) topography-dependent atmospheric signals: 031207-040215; (b) topography-independent atmospheric signals: 030406-030615.

ellite line of sight. The discontinuous map of phase differences is unwrapped to form a continuous map of the LOS range changes. Since the coherence is generally good (Figure 5) even for long-term pairs due to the arid climate, low relief variations and a lack of vegetation, the performance of phase unwrapping is quite robust, which was validated with a phase closure technique (Biggs et al. 2007) in this study. The basic idea of the phase closure technique is that the phase contributions behave in a conservative manner, i.e. $\phi_{ln} - \phi_{lm} - \phi_{mn} = 0$, where ϕ_{mn} is the phase contribution of interferogram mn constructed from acquisitions n and m . In contrast, phase unwrapping errors do not follow this rule so can be easily identified by summing around a loop and checking residuals (Biggs et al. 2007).

Atmospheric effect. A major source of error for repeat-pass InSAR is the phase delay in radio signal propagation through the atmosphere (especially the part due to tropospheric water vapour) (e.g. Figure 6). It is demonstrated that a better time series of post-seismic motion after the 2003 Bam (Iran) earthquake can be achieved after reduction of water vapour effects using an InSAR Time Series with a Precipitable Water Vapour correction model (InSAR TS + PWV) generated from coincident full resolution (0.3 km) MERIS near IR water vapour data (Li et al. 2009a). However, only reduced resolution (1.2 km) MERIS data is available over Tibet and the signals of interest have a comparable scale of (2 km × 3 km). Examination of the 90 small baseline interferograms reveals that water vapour effects are smaller than half a fringe in all cases, which is only one sixth of the uplift signals observed. Therefore, all 90 the small baseline interferograms can be effectively considered as

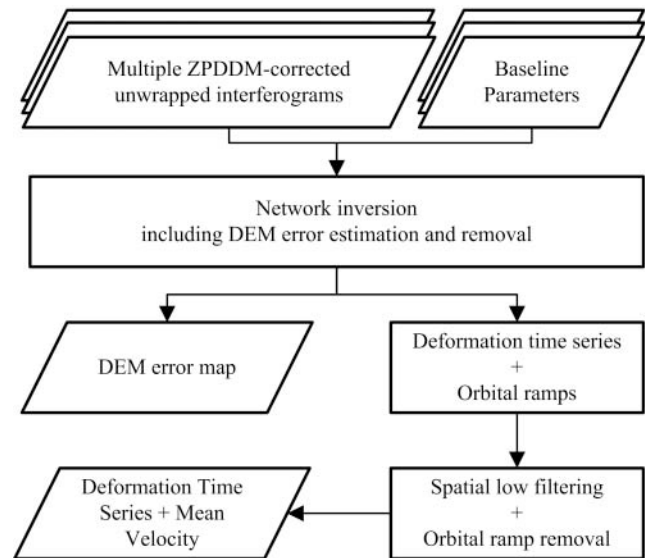


Figure 7: Flowchart of InSAR TS + PWV (Li et al. 2009a). Note: all the 90 small baseline interferograms used in this study can be effectively considered as ZPDDM-corrected interferograms due to their limited water vapour effects and the small area of the Huatugou oil field.

ZPDDM-corrected interferograms, and water vapour effects were considered as white noise in our InSAR time series.

3.2. InSAR time series results

Figure 7 shows the flowchart of the InSAR + PWV technique (Li et al. 2009a) used in this study. The InSAR + PWV technique allows us to map surface deformation as it evolves in time together with a

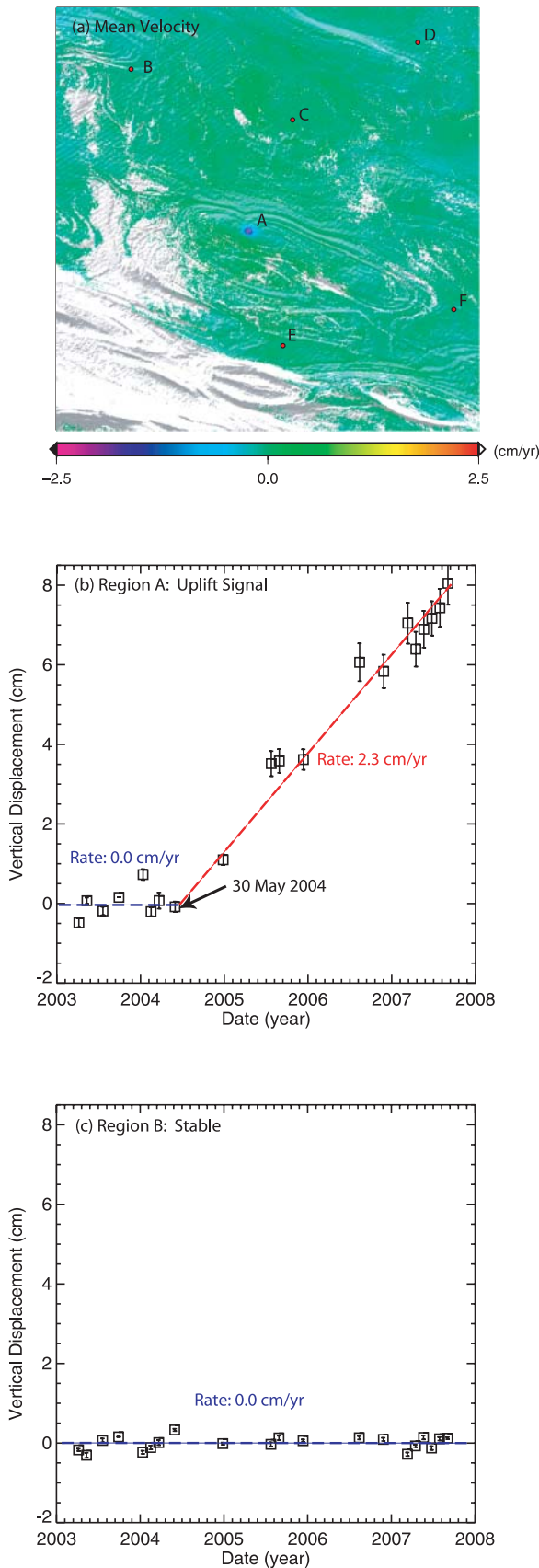


Figure 8: (a) Mean velocity over the region of interest during the period between 2003 and 2007. (b) Displacement time series over region A. Blue dashed line indicates the mean velocity from 06 April 2003 to 30 May 2004, whilst red dashed line represents the mean velocity between 30 May 2004 and 02 Sep 2007. (c) Displacement time series over region B. Blue dashed line indicates the mean velocity from 06 April 2003 to 02 Sep 2007. Note: *For simplicity*, the range changes in the satellite line of sight in Figures (b) and (c) are converted into the vertical direction by assuming no horizontal motion (though horizontal movements cannot be ruled out based on the available InSAR data only).

mean velocity field, with two key features: (1) no *a priori* deformation model is required in InSAR time series analysis, after water vapour correction is applied and/or when water vapour effects are limited; (2) the capability to provide spatially dense deformation maps is preserved by only using SAR pairs with small baselines.

Figure 8(a) shows the mean velocity of the study area during the period from 2003 to 2007. A maximum range change rate of ~ 2.2 cm/yr in the satellite LOS direction, corresponding to ~ 2.3 cm/yr of vertical deformation (assuming no horizontal motion), is observed in Region A (indicated by a red rectangle), whilst the rest of the region is relatively stable. On closer inspection of the InSAR-derived deformation time series over Region A, it is found that Region A did not start to uplift until May 2004, and that the uplift signal is nearly linear with a mean velocity of 2.3 cm/yr (Figure 8(b)). In contrast, the time series of Region B appears to be flat (i.e. the mean velocity is 0.0 cm/yr) (Figure 8(c)). It should be noted that similar patterns are observed in the time series over dozens of regions (e.g. C, D, E and F) that are almost evenly distributed across the whole area of interest.

In Figure 8(b), there is no obvious seasonal signal observed during the period from 30 May 2004 and 02 September 2007, indicating that it is unlikely that natural water recharging caused the uplift signal.

Examination of 2.5 m ALOS PRISM images reveals that there are several buildings (indicated by black arrowheads) and roads (indicated by red rectangles) around the nonlinear uplift signal (indicated by red circle) (Figure 9). It is also clear in Figure 9 that the uplift signal is located at a doubly-plunging anticline, which is a favoured location for oil and natural gas drilling. A phone investigation suggests that the uplift signal corresponds to the location of Huatugou Oil field where water injection has been employed since 2004 (Z. Xu, personal communication, 2008). Note that Bawden et al. (2001) reported that the Baldwin Hills oil fields in southern California uplifted at 5 ± 9 mm/yr because fluid injection had exceeded withdrawal since 1993. It appears that the Huatugou Oil field follows a similar uplift mechanism, that is, the observed uplift signal is more likely caused by water injection.

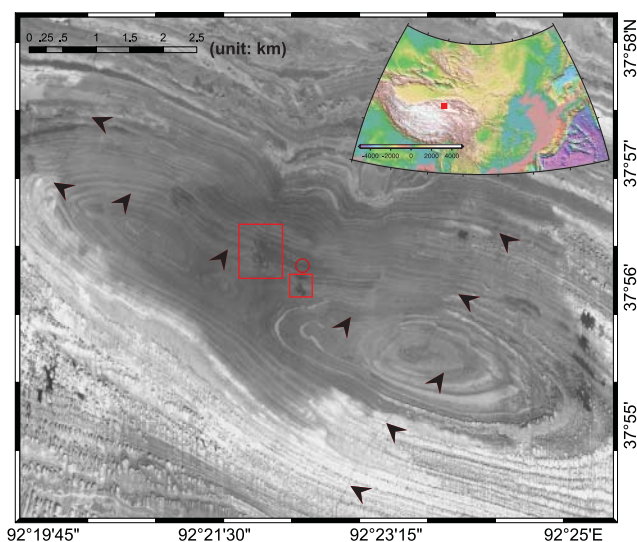


Figure 9: ALOS PRISM images of the region of interest with a pixel size of 2.5 m. Red circle: location of the uplift signal. Black arrowheads: locations of roads. Red rectangles: locations of buildings. Inset: location of the area within China.

4. Conclusions

In this paper, Small Baseline (SB) InSAR time series technique has been successfully employed to map ground motions of an area in Northern Tibet during the period between 2003 and 2007 using ENVISAT pairs with a perpendicular baseline (i.e. orbital separation) of less than 400 m. A nonlinear ground uplift motion was detected over the Huatugou oil field: the area of interest was relatively stable during the period from April 2003 to May 2004, whilst it has exhibited a nearly linear uplift since May 2004 with a total displacement magnitude of about 8 cm between May 2004 and September 2007. It should be noted that no deformation model was assumed in the InSAR time series analysis; therefore the consistency of the uplift rates between 2004 and 2007 not only suggests that the signal itself is ‘real’, but also indicates that SB InSAR can be employed for very precise deformation monitoring in oil fields.

It is also worth noting that the ground motion was “unexpected” in our study since our aim was to map the interseismic motion of the Eastern Altyn Tagh Fault. However, the overall nonlinear ground motion was easily observed when a time series analysis was performed, which shows the potential of SB InSAR as an early detection tool for surface deformations.

On the one hand, longer wavelength SAR data (e.g. L-band ALOS PALSAR) is available with better coherence (i.e. less temporal decorrelation) than C-band due to its capability to penetrate more deeply through vegetation. As a result, this makes InSAR deformation mapping possible over longer time intervals at wider scales than before. On the other hand, advanced InSAR techniques (e.g. InSAR time series) are being developed to combine multi-temporal,

multi-wavelength SAR data together for mapping time-variant ground surface deformation. Therefore, it is reasonable to believe that InSAR will become a practical deformation monitoring tool in the near future.

Acknowledgments

This work was carried out as part of the activities of the NERC Earth Observation Centre of Excellence: Centre for the Observation and Modelling of Earthquakes and Tectonics (COMET+), and partly supported by OPA Project 200705003 and NSFC Project 40576044. We are grateful to A. Sibthorpe, Eric Fielding and Zhong Lu for useful discussions. We thank JPL/Caltech for the use of the ROI_PAC software to generate our interferograms (Rosen et al. 2004). Figures 2–6 and 8(a) were prepared using the public domain Generic Mapping Tools (Wessel and Smith 1998). The ASAR data were supplied under ESA ENVISAT data grants C1P.2525 and C1P.3336.

References

- Bawden, G. W., Thatcher, W., Stein, R. S., Hudnut, K. W., and Peltzer, G., Tectonic contraction across Los Angeles after removal of groundwater pumping effects, *Nature* 412 (2001), 812–815.
- Berardino, P., Fornaro, G., Lanari, R., and Sansosti, E., A new algorithm for surface deformation monitoring based on small baseline differential SAR interferograms, *IEEE Transactions Geoscience and Remote Sensing* 40 (2002), 2375–2383.
- Biggs, J., Wright, T., Lu, Z., and Parsons, B., Multi-interferogram method for measuring interseismic deformation: Denali Fault, Alaska, *Geophysical Journal International* 170 (2007), 1165–1179.
- Bürgmann, R., Rosen, P. A., and Fielding, E. J., Synthetic Aperture Radar Interferometry to Measure Earth’s Surface Topography and Its Deformation, *Annual Review of Earth and Planetary Sciences* 28 (2000), 169–209.
- Casu, F., Manzo, M., and Lanari, R., A quantitative assessment of the SBAS algorithm performance for surface deformation retrieval from DInSAR data, *Remote Sensing of Environment* 102 (2006), 195–210.
- Chen, C. W. and Zebker, H. A., Network approaches to two-dimensional phase unwrapping: intractability and two new algorithms, *Journal of the Optical Society of America A-Optics Image Science and Vision* 17 (2000), 401–414.
- Ding, X.-L., Li, Z.-W., Zhu, J.-J., Feng, G.-C., and Long, J.-P., Atmospheric Effects on InSAR Measurements and Their Mitigation, *Sensors* 8 (2008), 5426–5448.
- Farr, T. G., Rosen, P. A., Caro, E., Crippen, R., Duren, R., Hensley, S., Kobrick, M., Paller, M., Rodriguez, E., Roth, L., Seal, D., Shaffer, S., Shimada, J., Umland, J., Werner, M., Oskin, M., Burbank, D., and Alsdorf, D., The Shuttle Radar Topography Mission, *Rev. Geophys.* 45 (2007), doi:10.1029/2005RG000183.
- Hanssen, R. F., *Radar interferometry: data interpretation and error analysis*, Kluwer Academic Publishers, Dordrecht, Netherlands, 2001.
- Janssen, V., Ge, L., and Rizos, C., Tropospheric corrections to SAR interferometry from GPS observations, *GPS Solutions* 8 (2004), 140–151.
- Lanari, R., Casu, F., Manzo, M., Zeni, G., Berardino, P., Manunta, M., and Pepe, A., An Overview of the Small Baseline Subset Algorithm: a DInSAR Technique for Surface Deformation Analysis, *Pure and Applied Geophysics* 164 (2007), 637–661.

- Lanari, R., Mora, O., Manunta, M., Mallorquí, J. J., Berardino, P., and Sansosti, E., A Small-Baseline Approach for Investigating Deformations on Full-Resolution Differential SAR Interferograms, *IEEE Transactions on Geoscience and Remote Sensing* 42 (2004), 1377–1386.
- Li, Z., Fielding, E. J., and Cross, P., Integration of InSAR time series analysis and water vapour correction for mapping postseismic deformation after the 2003 Bam, Iran Earthquake, *IEEE Transactions on Geoscience and Remote Sensing*, in press, 2009a.
- Li, Z., Fielding, E. J., Cross, P., and Muller, J.-P., Interferometric synthetic aperture radar atmospheric correction: GPS topography-dependent turbulence model, *Journal of Geophysical Research* 111 (2006a), doi:02410.01029/02005JB003711.
- Li, Z., Fielding, E. J., Cross, P., and Muller, J.-P.: Interferometric synthetic aperture radar atmospheric correction: MEdium Resolution Imaging Spectrometer and Advanced Synthetic Aperture Radar integration, *Geophysical Research Letters* 33 (2006b), doi:06810.01029/02005GL025299.
- Li, Z., Fielding, E. J., Cross, P., and Preusker, R., Advanced InSAR atmospheric correction: MERIS/MODIS combination and stacked water vapour models, *International Journal of Remote Sensing*, in press, 2009b.
- Li, Z., Muller, J.-P., Cross, P., Albert, P., Fischer, J., and Bennartz, R., Assessment of the potential of MERIS near-infrared water vapour products to correct ASAR interferometric measurements, *International Journal of Remote Sensing* 27 (2006c), 349–365.
- Li, Z., Muller, J.-P., Cross, P., and Fielding, E. J., Interferometric synthetic aperture radar (InSAR) atmospheric correction: GPS, Moderate Resolution Imaging Spectroradiometer (MODIS), and InSAR integration, *Journal of Geophysical Research* 110 (2005), doi:03410.01029/02004JB003446.
- Li, Z. W., Ding, X. L., and Liu, G. X., Modelling atmospheric effects on InSAR with meteorological and continuous GPS observations: algorithms and some test results, *Journal of Atmospheric and Solar-Terrestrial Physics* 66 (2004), 907–917.
- Lu, Z., Kwoun, O. and Rykhus, R., Interferometric synthetic aperture radar (InSAR): its past, present and future, *Photogrammetric Engineering and Remote Sensing* 73 (2007), 217–221.
- Massonnet, D., Feigl, K., Rossi, M., and Adragna, F., Radar interferometric mapping of deformation in the year after the Landers earthquake, *Nature* 369 (1994), 227–230.
- Massonnet, D. and Feigl, K. L., Radar interferometry and its application to changes in the Earth's surface, *Rev. Geophys.* 36 (1998), 441–500.
- Onn, F. and Zebker, H. A., Correction for interferometric synthetic aperture radar atmospheric phase artifacts using time series of zenith wet delay observations from a GPS network, *Journal of Geophysical Research* 111 (2006), doi:09110.01029/02005JB004012.
- Otten, M. and Dow, J., ENVISAT Precise orbit determination. 2004 Envisat & ERS Symposium, Salzburg, Austria, 2004.
- Rosen, P. A., Hensley, S., Peltzer, G., and Simons, M., Updated Repeat Orbit Interferometry package released, *EOS, TRANSACTIONS, American Geophysical Union* 85 (2004), 47.
- Xu, C. J., Wang, H., Ge, L. L., Yonezawa, C., and Cheng, P., InSAR tropospheric delay mitigation by GPS observations: A case study in Tokyo area, *Journal of Atmospheric and Solar-Terrestrial Physics* 68 (2006), 629–638.
- Zebker, H. A., Rosen, P. A., and Hensley, S., Atmospheric effects in interferometric synthetic aperture radar surface deformation and topographic maps, *Journal of Geophysical Research* 102 (1997), 7547–7563.

Received Aug 12, 2008

Accepted Mar 11, 2009

Author information

Zhenhong Li
COMET+
Department of Geographical and Earth Sciences
University of Glasgow
Glasgow G12 8QQ, United Kingdom
E-mail: zhenhong.li@ges.gla.ac.uk

Yanxiong Liu and Xinghua Zhou
Ocean Geomatics Center
The First Institute of Oceanography
State Oceanic Administration in China
Qingdao 266061, China

Paul Cross
COMET+
Department of Civil, Environmental and Geomatic Engineering
University College London
London WC1E 6BT, United Kingdom

Wanpeng Feng
Institute of Geophysics
China Earthquake Administration
Beijing 100081, China